

Global Stability and Tipping Point Prediction of the Coral Reef Ecosystem

Li Xu,¹ Denis Patterson,^{2,3} Simon Asher Levin,^{3,4, a)} and Jin Wang^{5, b)}

¹⁾State Key Laboratory of Electroanalytical Chemistry, Changchun Institute of Applied Chemistry, Chinese Academy of Sciences, Changchun, Jilin, 130022, P.R.China

²⁾Department of Mathematical Sciences, Durham University, Upper Mountjoy Campus, Stockton Road, Durham DH1 3LE, UK.

³⁾High Meadows Environmental Institute, Princeton University, Princeton, NJ 08544

⁴⁾Department of Ecology and Evolutionary Biology, Princeton University, Princeton, NJ 08544

⁵⁾Department of Chemistry and of Physics and Astronomy, State University of New York at Stony Brook, Stony Brook, NY 11794-3400, USA.

(Dated: 8 March 2024)

Coral reefs are highly diverse and important marine ecosystems, with the potential for multiple stable states and critical transitions between alternative states. Using landscape-flux theory, we explore the dynamics of these systems in the face of stochastic perturbations. We quantified the average flux as the non-equilibrium driving force and the entropy production rate as the nonequilibrium thermodynamic cost. We also compute the nonequilibrium free energy and time irreversibility from the cross-correlation functions as early warning signals for critical transitions. These early warning signals, characterized by turning points in the middle of two bifurcations, can provide predictions for both left and right bifurcations, much earlier than critical slowing down, a more traditional indicator that is evident only closer to the bifurcation point(s).

Keywords: landscape, flux, non-equilibrium, coral reef, early warning signal

I. INTRODUCTION

~~The most famous of all coastal ecosystems are coral reef ecosystems, which have very rich biodiversity.~~ Complex coral reef systems have significant functionality and commercial value for coastal protection, and maintenance of fish and marine biodiversity¹⁻⁴. Yet coral reefs around the world face a number of issues and are under severe threat to abundance, diversity, habitat structure and function⁵⁻⁸. Coral reef degradation is the result of a combination of human activities (e.g. overfishing, pollution) and natural disasters (e.g. disease, hurricanes, bleaching). Average hard coral cover in the Caribbean Basin dropped from around 50% to 10% during only three decades from 1977^{9,10}. Although algal blooms do not usually kill corals directly, algae competes with coral for space and light, leading to the death of older corals. In the process, the algae inhibit the ability of new corals to grow, which in turn reduces the ability of coral populations to recover from environmental threats. Ultimately, algae control the entire ecosystem. The most dramatic transformation is that of Caribbean reefs to a very different state covered in algae⁵⁻⁸.

Human land use increases ocean nutrient loading, which promotes the growth of algae. Herbivorous fish have been controlling algal biomass ~~for a long time~~^{5,6}. However, overfishing of various fish species has reduced herbivorous fish such as parrotfish. Parrotfish are abundant herbivores that feed primarily on algae, and they can indirectly benefit corals by reducing the competition of algae. Management efforts to increase parrotfish populations are believed to be critical to maintaining resilient, coral-dominated reefs^{5,6}. Protecting parrot fish is ecologically important for endangered

Caribbean corals. Parrotfish communities can maintain about 40% of coral reefs under permanent grazing, but overfishing reduces this capacity to about 5%.⁵⁻⁸ A moderate sea urchin population is a more effective herbivore than parrotfish. For example, an algal dominated state replaced the coral-dominated original state in 1983 following mass sea urchin die-offs, leaving only the less effective grazer, the parrotfish. Coral reef systems in the Caribbean have two steady states: algal-dominated state and coral-dominated state⁵⁻⁸.

The critical transition scenario of the coral-algal model has been discussed by many researchers^{1-6,8}. A more complex model including the importance of recruitment seasonality and grazing influence has been explored recently⁷. At the level of low grazing rate in which parrotfish graze macroalgae without distinction from algal turfs, the coastal seabed is covered by macroalgae, showing a macroalgal-dominant state. At high levels of the grazing rate, the coastal seabed is covered by coral, showing a coral-dominant state. Once the grazing rate in the water decreases from high level below a certain threshold, the coral will disappear, the macroalgae will grow in large quantities, and the coastal seabed will change from the coral-dominant state to the macroalgal-dominant state⁵⁻⁷. Within a certain grazing rate range, the macroalgal-dominant state and coral-dominant state represent alternative stable states¹⁻⁷.

State changes in complex systems can be described formally in terms of phase transitions or bifurcations. Nonlinear dynamical systems can have steady states, periodic orbits, and even more complex chaotic dynamics. However, most studies have focused on the stability of ecological systems at equilibrium and then explored the respective basins of attraction of the equilibria in different parameter regimes, an approach that focuses on the local stability near the equilibrium points¹¹. Global stability analysis of the coral-algal systems is challenging and the link between the global characterization of the coral-algal systems and the dynamics

^{a)}Electronic mail: slevin@princeton.edu

^{b)}Electronic mail: jin.wang.1@stonybrook.edu

of elements is not thoroughly understood. We will show how the landscape-flux theory from non-equilibrium statistical mechanics can provide a powerful framework to study the global stability of the coral reef system. We use a typical coral-algal model as a case study^{5,6}.

It is very important to understand the response mechanisms and critical thresholds of natural systems to human disturbance and to carry out early warning prevention and control. Exploring the tipping points in complex systems and anticipating critical transitions has become more and more significant in ecological systems already experiencing stressors due to climate change. Recent theoretical and empirical research on the underlying instabilities of ecological systems has been concerned with the development of early warning signals of ecological catastrophes (typically associated with a phase transition or bifurcation). Most of the studies are based on one dimensional stochastic dynamical models, which are often general equilibrium systems. Critical slowing down theory is used widely for predicting the early warning signals from observed univariate time series. As the control parameter approaches a critical parameter value, the dynamics of a complex system slows down and the current steady state loses its stability¹²⁻¹⁷. The general early warning signals of critical slowing down from time series data are often expressed in terms of greater variance, autocorrelation, and return time by the perturbation. Critical slowing down can often be used successfully as an early warning signal in one-dimensional systems.

Early warning signals of critical transitions help us to anticipate and understand the likelihood of abrupt and significant changes in complex systems. Ecosystems can usually maintain a sustainable balance before reaching a critical point, but upon crossing the critical point, the current stable state can lose stability, triggering a catastrophic transition to a new stable state. Near the critical point, the mechanisms sustaining the functioning of the ecosystem can break down, resulting in a sudden loss of resilience and preventing recovery. It is crucial to detect signals of critical transition as early as possible to give enough time to avert a potential ecological crisis, and the search for early predictions of imminent structural changes has thus become the focus of intense research. Critical slowing down theory is among the most popular and well-known approaches, but its predictions are only valid near the bifurcation point. In the context of coastal ecosystems, we aim to detect early warning signals of critical transitions from a socially-valued state, like a coral-dominated state, to a "disaster" stable state, like a macroalgal-dominated reef. Moreover, we also want to assess the likelihood of the reverse transition from a disaster stable state to a socially-valued stable state. Thus, it will be of great practical significance if we can predict both the impending transition to the disaster state or the impending recovery to the socially-valued state by extracting the early warning signals before the critical transition occurs.

Researchers have come to recognize that ecological systems should be treated as complex systems, which are inherently multivariate. Our understanding of high dimensional complex dynamic behavior of ecological

systems still requires further development¹⁶⁻²⁰. It may be that something is missing from these conventional one dimensional stochastic dynamic ecological models, preventing us from describing the behavior generated by the rotational curl force among the variables. Unlike traditional ecological theories under the assumption of general equilibrium, we should describe ecological systems under non-equilibrium processes. Recent advances in nonequilibrium statistical mechanics can provide insights into the understanding of the formation and the stability of attractor states, bifurcations and catastrophe in phase transitions of the physical and biological systems²¹⁻³¹.

In this study, we use the entropy production rate to quantify the thermodynamic cost, average flux to quantify the dynamical driving force and the average difference in cross correlations between the forward in time and the backward in time to quantify the time irreversibility of the time series as the new early warning signals for the phase transitions or bifurcations of the high dimensional complex ecological system. We found that our nonequilibrium warning indicators with their turning points being in the middle of two bifurcations can provide the predictions for both bifurcations, which are much earlier than the predictions given by the critical slowing down near the bifurcations. The potential-flux landscape theory provides new way of exploring the underlying mechanisms causing ecological catastrophes.

II. METHODS

A. Model of Coral-Algal Model

We explore the dynamics of a typical coral reef ecosystem model^{5,6}, whose schematic diagram is shown in Fig. 1 below. Our ecosystem model contains three functional types: Macroalgae (X), coral (Y), and algal turfs (T), entities that can be colonised by either macroalgae or coral. We track the evolution of the proportions of space occupied by each functional type, effectively assuming that the system is spatially well-mixed, leading to a spatially implicit modelling framework. Corals recruit and overgrow algal turfs at rate r , while coral can be overgrown by macroalgae at rate a . Natural coral mortality occurs at rate h and we assume that space released by the death of the coral will be rapidly recolonized by algal turfs. Macroalgae colonizes algal turfs by covering them vegetatively at rate γ . Reef grazers, such as parrotfish, are assumed to consume macroalgae and algal turfs equally at rate g , and algal turfs arise when macroalgae are grazed. Thus the rate of algal turf production as a function of macroalgae is given by the proportion of grazing that affects macroalgae, i.e. $gX/(X+T)$ ⁵⁻⁷.

The coral reef system can thus be described by the following set of nonlinear ordinary differential equations (ODEs):

$$\begin{aligned}\frac{dX}{dt} &= aXY - \frac{gX}{X+T} + \gamma XT \\ \frac{dY}{dt} &= rTY - hY - aXY\end{aligned}\quad (1)$$

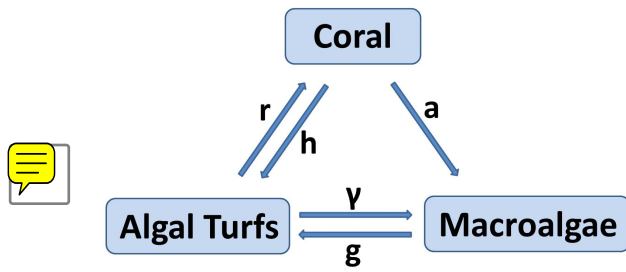


FIG. 1. The schematic diagram for coral reef model.

Symbol	Ecological interpretation	Default value
a	the rate that corals are overgrown by macroalgae	0.1
γ	the rate that macroalgae spread vegetatively over algal turfs	0.8
r	the rate that corals recruit to and overgrow algal turfs	1.0
h	the natural mortality rate of corals	0.44

TABLE I. Parameters interpretation and default values^{5,6}

where X represents the proportion of space covered by macroalgae and Y represents the proportion of space covered by coral. T represents the proportion of algal turf cover and since we assume that all space (seabed) is completely covered by either macroalgae, coral or algal turfs, we have $X + Y + T = 1$, or $T = 1 - X - Y$. g is the grazing rate that parrotfish graze macroalgae without distinction from algal turfs range from 0 to 0.8. The parameter interpretations and their default values are given in [Table I](#) below.

B. Landscape and flux theory for the coral reef model

The dynamics of the coral reef model without noise or external forcing are described by the set of ordinary differential equations (1). In practice, coral reef ecosystems are subject to multifarious noise; internal stochasticity may arise due to variations in individual growth rates or grazer patterns, while there may also be substantial external forcing from processes such as ocean acidification, sedimentation or other climate change driven stressors. Our original deterministic model (1) can be rewritten in differential notation as $d\mathbf{x} = \mathbf{F}(\mathbf{x})$, where the vector \mathbf{x} represents the current state of the ecosystem and the "driving force" \mathbf{F} captures the set of interactions and transitions between the coral, macroalgae and algal turfs outlined above, i.e. the right-hand side of the ODEs (1). To extend our model to capture the impact of different sources of noise on the dynamics, let

$$d\mathbf{x} = \mathbf{F}(\mathbf{x})dt + \mathbf{m} \cdot d\mathbf{W}, \quad (2)$$

where \mathbf{W} , coupled with the matrix \mathbf{m} , represents an independent Gaussian noise process^{22,32,33}. It is convenient to let $D\mathbf{G} = (1/2)(\mathbf{m} \cdot \mathbf{m}^T)$ so that D is a constant representing the scale of the fluctuations and \mathbf{G} is the diffusion matrix of the stochastic fluctuations. We assume throughout that \mathbf{G} is a diagonal identity matrix for simplicity; allowing non-trivial off-diagonal entries introduces correlated noise impacts on

the model and considerably increases the complexity of the subsequent analysis.

The probability of finding the coral reef system in state \mathbf{x} at time t in our stochastic model (2) is given by the probability density function $P(\mathbf{x}, t)$, which solves the associated Fokker-Planck (partial differential) equation^{22,34,35}:

$$\partial_t P = -\nabla \cdot \mathbf{J} = -\nabla \cdot [\mathbf{F}P - (1/2)\nabla \cdot ((\mathbf{m} \cdot \mathbf{m}^T)P)], \quad (3)$$

where \mathbf{J} denotes the flux of the system.

We can obtain the steady-state (stationary) probability distribution $P_{ss}(\mathbf{x})$ by solving the steady-state Fokker-Planck equation:

$$0 = -\nabla \cdot \mathbf{J}(\mathbf{x}) = -\nabla \cdot [\mathbf{F}(\mathbf{x})P_{ss}(\mathbf{x}) - (1/2)\nabla \cdot ((\mathbf{m} \cdot \mathbf{m}^T)P_{ss}(\mathbf{x}))], \quad (4)$$

We may look for a so-called "detailed balance solution" to equation (4) in which the flux \mathbf{J} is zero; this corresponds to an equilibrium system with no net input or output. In this equilibrium setting, the steady-state probability distribution is given by $P_{ss} \sim \exp[-U]$ ^{22,32,34,35}, where U is called the population-potential landscape. In equilibrium systems, we can decompose the driving force \mathbf{F} as:

$$\mathbf{F} = -D\mathbf{G} \cdot \nabla U + D\nabla \cdot \mathbf{G} \quad (5)$$

and thus \mathbf{F} is determined by the gradient of the population-potential landscape. We may calculate or experimentally estimate the distribution P_{ss} under fluctuations by solving equation (4) above or collecting statistics from experiments.

We can then obtain the population potential landscape U via formula: $U = -\ln P_{ss}$ ^{22,23,34}. For nonequilibrium system, force \mathbf{F} can be decomposed as:

$$\mathbf{F} = -D\mathbf{G} \cdot \nabla U + D\nabla \cdot \mathbf{G} + \mathbf{J}_{ss}/P_{ss}, \quad (6)$$

where \mathbf{J}_{ss} denotes the non-zero steady-state probability flux. The steady-state flux is given by $\mathbf{J}_{ss} = \mathbf{F}P_{ss} - D\nabla \cdot (\mathbf{G}P_{ss})$. The steady-state probability flux satisfies the divergence-free condition $\nabla \cdot \mathbf{J}_{ss} = 0$, meaning that the final term on the right-hand side of (6) is a purely rotational component of the driving force. The gradient of the potential, $-D\mathbf{G} \cdot \nabla U$, pushes the system towards stable states, while the (divergence free) flux component creates a rotational flow on the system and promotes transitions between alternative stable states. In the nonequilibrium case, the population-potential landscape U and the flux \mathbf{J}_{ss} both contribute to the driving force \mathbf{F} of the dynamics. The population-potential landscape, U , despite being effectively an equilibrium quantity, can give us valuable information about the global stability of nonequilibrium systems, as we will demonstrate presently for our coral reef model.

In the nonequilibrium case, the non-zero curl flux \mathbf{J}_{ss} breaks the detailed balance and thus provides a direct quantitative measurement of how far the system is from equilibrium^{21-23,25-27}. By measuring how far the system is from equilibrium we can investigate the onset of an instability in the current state and detect the creation of or transition to a new stable state. The flux will therefore be a key component in developing our early warning indicators for nonequilibrium

systems. More concretely, the flux provides a basis for studying the nonequilibrium thermodynamics of the system in terms of the entropy production. The entropy of the stochastic system (2) can be defined as $S_{entropy} = -\int P \ln P d\mathbf{x}$ for the stochastic system. The change of the entropy in time can be decomposed into the entropy production rate (EPR) and heat dissipation rate:

$$\dot{S}_{entropy} = \dot{S}_{EPR} - \dot{S}_e, \quad (7)$$

where the entropy production rate is $EPR = \dot{S}_{EPR} = \int d\mathbf{x} (\mathbf{J} \cdot (D\mathbf{G})^{-1} \cdot \mathbf{J}) / P^{23,36-38}$, where \dot{S}_{EPR} is the rate of the system entropy change while \dot{S}_e is the rate of the environment entropy change which is also the heat dissipation rate $\dot{S}_e = \int d\mathbf{x} (\mathbf{F} - D\nabla \cdot \mathbf{G}) \cdot \mathbf{J}$. The EPR is directly related to the flux \mathbf{J} and a larger flux gives rise to a higher EPR and hence more deviations away from equilibrium. When the system is at a steady-state, the EPR and the heat dissipation rate are equal^{23,36-38}. We will use both the EPR and the average flux $Flux_{av} = \int |\mathbf{J}| d\mathbf{x}$ to measure the non-equilibriumness and generate early warning signals of critical transitions in the stochastic coral reef model (2).

Lyapunov function for the coral reef model under zero fluctuations

In deterministic dynamical systems Lyapunov functions are a powerful tool for studying for stability analysis as they enable a characterization of the global stability of an attractor, as opposed to the weaker information obtained via a local stability analysis. There is no general method for constructing Lyapunov functions for complex nonlinear systems, even in the deterministic case, but we can in fact use the steady state probability distribution P_{ss} and the population potential U to explore the global stability of (2) under finite fluctuations. Unfortunately, the population-potential landscape U is not a Lyapunov function for the system (2) in general^{37,39}. In the limit of small noise ($D \rightarrow 0^+$), it can however be shown that the so-called intrinsic potential landscape, ϕ_0 , is a Lyapunov function (see Appendix for details?). We can compute ϕ_0 by solving the Hamilton-Jacobi equation:

$$H = \mathbf{F} \cdot \nabla \phi_0 + \nabla \phi_0 \cdot \mathbf{G} \cdot \nabla \phi_0 = 0. \quad (8)$$

The Hamilton-Jacobi equation (8) results from expanding the population potential U in powers of D (the noise level), plugging this series into the Fokker-Planck equation (4) and truncating at order D^{-1} to obtain the equation for ϕ_0 .^{22,37,39}

To see that ϕ_0 is indeed a Lyapunov function for the system (2), calculate as follows using (2) and (8):

$$\frac{d}{dt} \phi_0(\mathbf{x}) = \dot{\mathbf{x}} \cdot \nabla \phi_0 = \mathbf{F} \cdot \nabla \phi_0 = -\nabla \phi_0 \cdot \mathbf{G} \cdot \nabla \phi_0 \leq 0,$$

where the last inequality holds provided that \mathbf{G} is a positive definite matrix. Therefore $\phi_0(\mathbf{x})$ monotonically decreases along the deterministic trajectory in the zero fluctuation limit, i.e. as $D \rightarrow 0^+$. Therefore, ϕ_0 can be used to quantify the global stability of the system in the small noise regime. In addition, the intrinsic potential landscape ϕ_0 is associated

with the steady-state probability and population potential landscape via the formula $U = -\ln P_{ss} \sim \phi_0/D$ as $D \rightarrow 0^+$.

The driving force \mathbf{F} in the zero fluctuation limit can be decomposed into a gradient term and a curl term:

$$\mathbf{F} = -\mathbf{G} \cdot \nabla \phi_0 + (\mathbf{J}_{ss}/P_{ss})|_{D \rightarrow 0} =: -\mathbf{G} \cdot \nabla \phi_0 + \mathbf{V}.$$

The first term $-\mathbf{G} \cdot \nabla \phi_0$ represents the gradient of the non-equilibrium intrinsic potential and we define the quantity $\mathbf{V} = (\mathbf{J}_{ss}/P_{ss})|_{D \rightarrow 0}$ to be the intrinsic steady-state flux velocity. The second term $\mathbf{J}_{ss}|_{D \rightarrow 0}$ represents the steady-state intrinsic flux and is divergence free due to the equation $\nabla \cdot \mathbf{J} = 0$. The relationship between ϕ_0 and the intrinsic flux is given by $(\mathbf{J}_{ss}/P_{ss})|_{D \rightarrow 0} \cdot \nabla \phi_0 = \mathbf{V} \cdot \nabla \phi_0 = 0$ from the Hamilton-Jacobi equation. Thus, we can conclude that the gradient of the intrinsic potential is perpendicular to the intrinsic flux in the zero fluctuation limit.

The intrinsic potential ϕ_0 is difficult to calculate for the coral reef model (2) since the state space is an isosceles triangle ($0 < X, Y < 1, 0 < 1 - X - Y < 1$). We expand the potential $U(\mathbf{x})$ in the small diffusion limit as $U(\mathbf{x}) = \phi_0(\mathbf{x})/D + \phi_1(\mathbf{x}) + O(D^2)$. We then use the linear fitting method to approximately solve for ϕ_0 by plotting the diffusion coefficients D versus DU . In the results shown below, we use data with small D and obtain the line of diffusion coefficient D versus $D \ln P_{ss}$, the slope of this line then gives the value of ϕ_0 .^{30,31,37}

We also discuss the non-equilibrium thermodynamics, entropy, energy and free energy of the general dynamical systems under the zero-fluctuation limit and the finite fluctuations and kinetic speed and dominant paths between the *Macroalgae* state and the *Coral* state in the SI.

III. RESULTS

We now explore the coral-algal model under finite and zero fluctuations using the landscape-flux approach outlined above. *Macroalgae* denotes the macroalgal-dominated state with low density of coral, while *Coral* denotes the coral-dominated state with low density of macroalgae.

Figure 2A shows the deterministic phase diagram as a function of g , the rate at which parrotfish graze macroalgae (without distinction from algal turfs). There are two stable states *Macroalgae* and *Coral* for a range of grazing rate g in the figure, the bistable region begins and ends with transcritical bifurcations. These transcritical bifurcations coincide with one of the equilibrium solutions entering or leaving the feasible region of the phase space (i.e. $0 \leq X + Y + T \leq 1, 0 \leq X, Y, T \leq 1$). We solve the Fokker-Planck equation of the coral reef model to obtain the steady state probability and thus the population landscape by the relationship: $U = -\ln P_{ss}$. Figure 3 shows three-dimensional population-potential landscapes (U) under finite fluctuations $D = 0.0005$. In Figure 3, the population-potential landscape initially has one stable state that evolves from the *Macroalgae* state with lower grazing rate g to the *Coral* state with increasing grazing rate g . As the grazing rate g increases further, the stable *Coral* state emerges. As the grazing rate

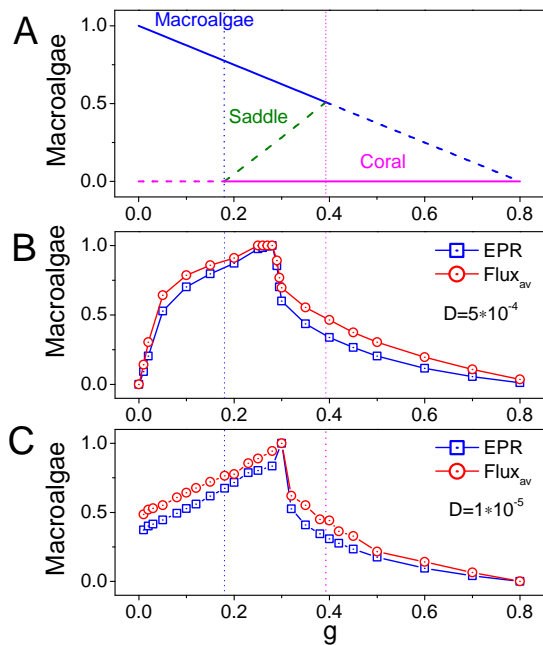


FIG. 2. A: The phase diagram versus grazing rate g . B: The population entropy production rate and the population average flux versus grazing rate g with $D = 5 \times 10^{-4}$. C: The population entropy production rate and the population average flux versus grazing rate g with $D = 1 \times 10^{-5}$.

g increases, the coral reef system switches from *Macroalgae* state with macroalgae dominant to *Coral* state with coral dominant (also shown in Figure 1A), and as grazing rate g increases further, the macroalgae almost disappears by the high grazing rate level. Eventually, the *Coral* state becomes dominant while the *Macroalgae* state disappears.

Disturbances and random fluctuations are almost inevitable for real ecosystems. If a system has two alternative stable states and the fluctuation intensity is large enough, the system can be driven from the local stable basin through the unstable steady state, to fall into the basin of attraction of another stable state. We can use the “ball-in-the-valley” conceptual model to describe this steady-state transition visually shown in Figure 4^{40,41}. Figure 4 shows the population potential landscape U projected on X with increasing grazing rate g . The potential landscape is quantified by the steady probability distribution of the stochastic coral-algal model. A ball represents the system, which tends to move downhill and is stabilized in the deep basins with different g . The valley characterizes the attraction basin in the dynamical system^{18–20}. The system subjected to small fluctuations can deviate from the steady state, the ball can climb up the hillside and the ball can return to its steady state at the bottom under small fluctuations. On the other hand, the ball may cross the ridge passing an unstable saddle point into the other stable valley (steady-state basin) with large enough fluctuations. We can see the M valley for *Macroalgae* is the only valley at $g = 0.125$; and the C valley for *Coral* is shallower than that of M valley at $g = 0.275$; the M valley and C valley have similar depth at $g = 0.3$; the C valley for *Coral* is deeper than that of M valley

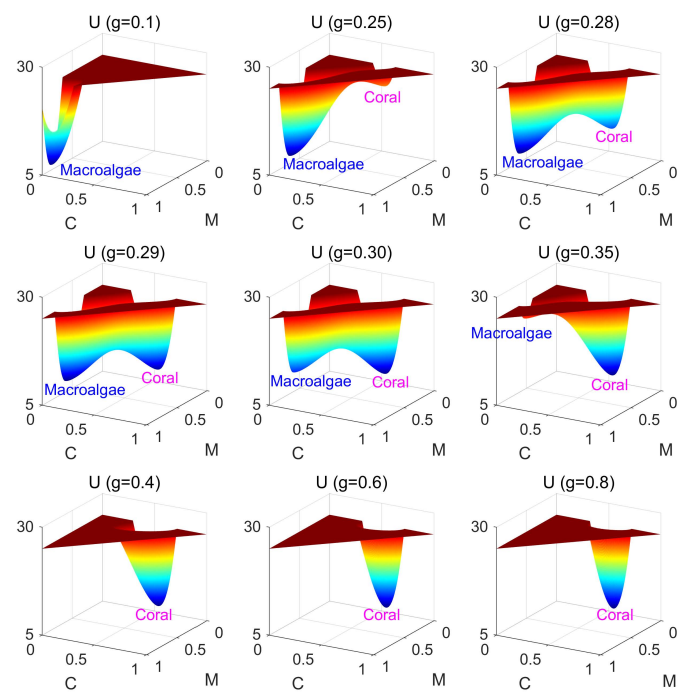


FIG. 3. The population potential landscape U for the coral reef model with finite fluctuation $D = 5 \times 10^{-4}$.

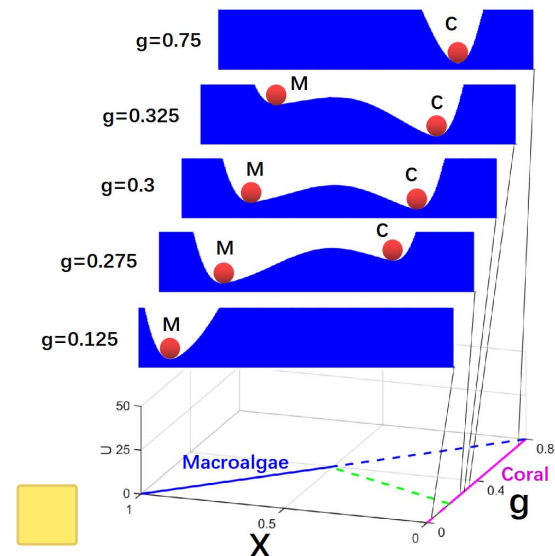


FIG. 4. The population potential landscape U projected on X .

at $g = 0.325$; the C valley for *Coral* is the only valley at $g = 0.75$.

Figure S1 shows the intrinsic potential landscape with different g for the coral reef model. We observe that the intrinsic potential landscapes are qualitatively similar to the corresponding population potential landscapes.

Figure 5A shows the intrinsic flux (white arrow) and the negative gradient of the intrinsic potential landscape (black arrow) at $g = 0.29$. We show the directions of larger values of

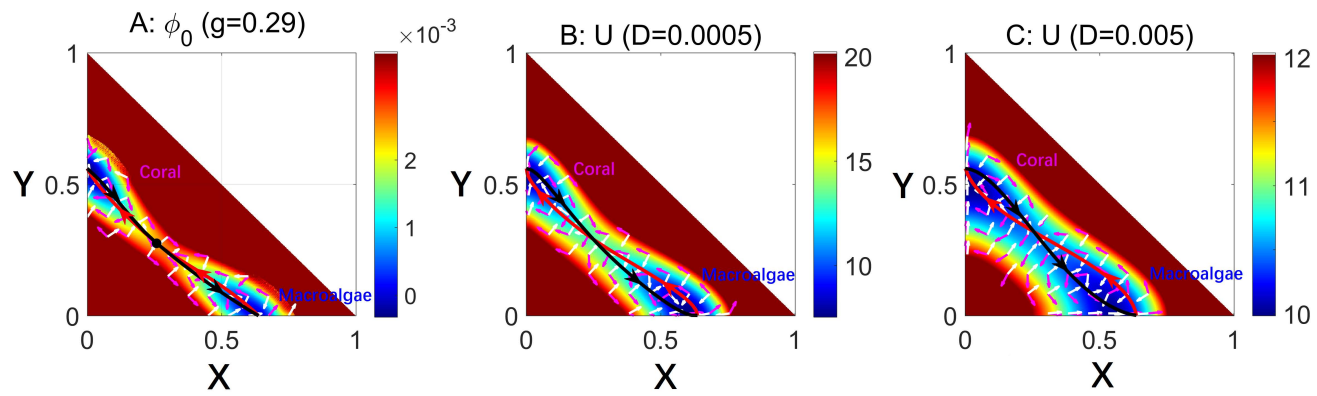


FIG. 5. The dominant intrinsic paths and fluxes on the intrinsic-potential landscape ϕ_0 with zero fluctuation limit and grazing rate $g = 0.29$ (A). The dominant population paths and fluxes on the population-potential landscape U with the diffusion coefficient $D = 0.0005$ (B), $D = 0.005$ (C). The red lines represent the dominant paths from the *Macroalgae* state to *Coral* state. The black lines represent the dominant paths from the *Coral* state to *Macroalgae* state. The white arrows represent the steady-state probability fluxes.

flux and the directions of the negative gradient of the intrinsic potential landscape around the steady state clearly.

The intrinsic fluxes are perpendicular to the negative gradients of the intrinsic potential landscape $-\nabla\phi_0$. This is because $(\mathbf{J}_{ss}/P_{ss})|_{D \rightarrow 0} \cdot \nabla\phi_0 = \mathbf{V} \cdot \nabla\phi_0 = 0$ due to the Hamilton-Jacobi equation, which is under the zero fluctuation limit. Figures 5B and C show the flux (white arrows) and negative gradient of the population potential landscape (black arrows) on the landscape for $D = 0.0005$ (B) and $D = 0.005$ (C). The fluxes originated from the grazing rate going around the stable states can increase the communications between the two stable states *Macroalgae* and *Coral*. In Figure 5, the negative gradient of the population-potential landscapes or the intrinsic potential landscape and the non-zero flux or intrinsic flux are the driving forces of the coral-algal system since the total force can be decomposed as: $\mathbf{F} = -D \cdot \nabla U + \mathbf{J}_{ss}/P_{ss} + D\mathbf{V} \cdot \mathbf{G}$ for finite fluctuations and $\mathbf{F} = -\mathbf{G} \cdot \nabla\phi_0 + (\mathbf{J}_{ss}/P_{ss})|_{D \rightarrow 0} = -\mathbf{G} \cdot \nabla\phi_0 + \mathbf{V}$ for zero fluctuation limit.

Figure 5 also shows the dominant population paths and the dominant intrinsic paths on the intrinsic potential landscape ϕ_0 under zero fluctuations limit (A) and the population-potential landscape U under finite fluctuations (B) and (C). The red lines denote the dominant intrinsic path(A) and dominant population path(BC) from *Macroalgae* state to *Coral*, while the black lines is the dominant intrinsic path(A) and dominant population path(B) from *Coral* state to *Macroalgae*. The purple arrow fluxes guide the dominant intrinsic paths in Figure 5A under zero fluctuations, which deviate from the steepest descent path and apart from each other passing through the saddle point in the equilibrium case under zero flux. The purple arrow fluxes guide the dominant population paths on the population-potential landscape under finite fluctuations in Figure 5BC, which also deviate from the steepest descent path. Therefore, under the limited fluctuations caused by non-zero flux, the dominant population path from *Macroalgae* to *Coral* and the dominant population path from *Coral* to *Macroalgae* are distinct. The dominant intrinsic path from *Macroalgae* to *Coral* and the dominant intrinsic path from *Coral* to *Macroalgae* are closer to each

other due to non-zero intrinsic flux under the zero limit fluctuation. The dominant path is thus irreversible and follows different paths due to the existence of the nonequilibrium rotational flux. The spiral shape of flux around the basins gives the origin of non-equilibrium dynamic features.

We show the barrier heights of the population-potential landscape and the barrier heights of the intrinsic potential landscape versus g in Figure 6A and B. The coral-algal system switches from *Macroalgae* state dominance to *Coral* state dominance with increasing g . Population barrier height $\Delta U_{SC} = U_S - U_C$ and intrinsic barrier height $\Delta\phi_{0SC} = \phi_{0S} - \phi_{0C}$ increase, while $\Delta U_{SM} = U_S - U_M$ and $\Delta\phi_{0SM} = \phi_{0S} - \phi_{0M}$ decrease as g increases, where U_S and ϕ_{0S} are the values of population potential and intrinsic potential at saddle point between *Macroalgae* state and *Coral* state, U_M and ϕ_{0M} are the minimum values of population potential and intrinsic potential in *Macroalgae* state, U_C and ϕ_{0C} are the minimum values of the population potential and the intrinsic potential in *Coral* state. As the parrotfish grazing rate increases, the *Macroalgae* state becomes less stable, while the *Coral* state becomes more and more stable. It is difficult to escape from the attraction of the more stable and deeper basin state to the other due to the higher barrier heights. Both the barrier heights and the intrinsic barrier heights have almost the same tendencies in Figure 6A and B as g increases.

Figure 6C shows the Mean first passage time (MFPT) which represents the average time for a stochastic process to reach a given state for the first time. One can quantify the kinetic speed or kinetic time by MFPT from one state to another. MFPT can be obtained from the following equation³⁴: $\mathbf{F} \cdot \nabla\tau + D\nabla^2\tau = -1$, where τ_{CM} represents the mean first passage time from state *Coral* to state *Macroalgae* and τ_{MC} represents the mean first passage time from state *Macroalgae* to state *Coral*. We show the logarithm of MFPT versus the population barrier heights in Figure 6C and observe that both $\ln\tau_{CM}$ and $\ln\tau_{MC}$ increases as the population barrier height increases. This implies that $\ln\tau$ and the barrier height have a relationship as $\tau \sim \exp(\Delta U)$. The escape time is longer for the system going out from one basin with higher barrier

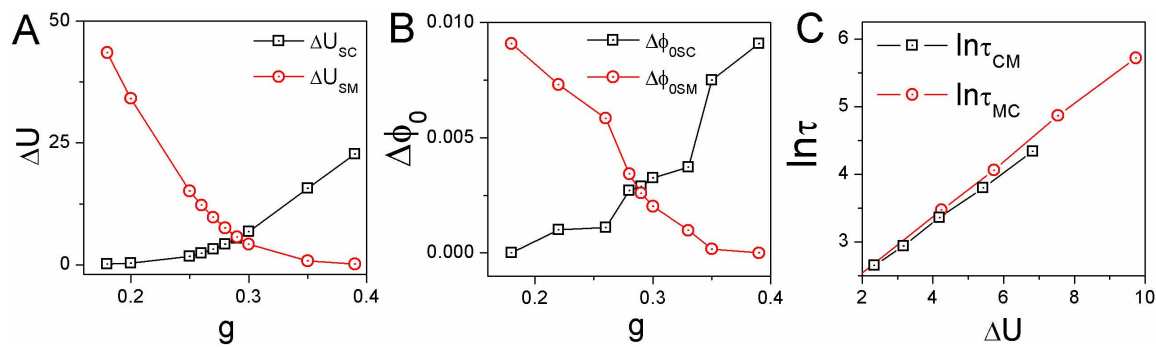


FIG. 6. A: The population barrier heights versus parameter g . B: The intrinsic barrier heights versus parameter g . C: The population barrier heights versus the mean first passage time. Population barrier height $\Delta U_{SC} = U_S - U_C$ and intrinsic barrier height $\Delta\phi_{0SC} = \phi_{0S} - \phi_{0C}$, $\Delta U_{SM} = U_S - U_M$ and $\Delta\phi_{0SM} = \phi_{0S} - \phi_{0M}$ and τ_{CM} represents the mean first passage time from state *Coral* to state *Macroalgae* and τ_{MC} represents the mean first passage time from state *Macroalgae* to state *Coral*.

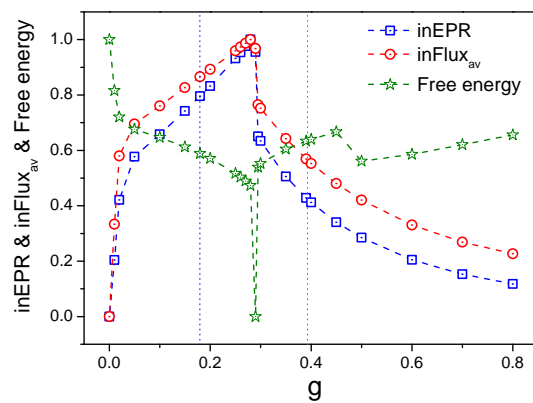


FIG. 7. The intrinsic entropy production rate, the population average flux and the free energy versus grazing rate g for the coral reef model.

height. The kinetic speed of the state switching is correlated to the population-potential landscape topography in terms of the barrier heights.

Figure 2BC shows the population entropy production rate EPR and the population average flux $Flux_{av}$ versus g under finite fluctuations $D = 0.0005$ and $D = 0.00001$. Figure 7 shows the intrinsic entropy production rate $inEPR$, the intrinsic average flux $inFlux_{av}$ versus g . We can see that as g increases, population EPR , population $Flux_{av}$, intrinsic $inEPR$, intrinsic $inFlux_{av}$ all increase first and then decrease, which undergo significant changes between the two transcritical bifurcations in Figure 2A. The peaks are distinct close to the phase transition between the two transcritical bifurcations from *Macroalgae* state to *Coral* state. We also show the intrinsic free energy in Figure 7. We can see that the intrinsic free energy has a minimum near the peaks of $inEPR$ and $inFlux_{av}$. Thus, one can use EPR and $Flux_{av}$, $inEPR$ and $inFlux_{av}$ and intrinsic free energy as indicators for the phase transitions and bifurcations of the coral-algal system.

We can explore the time irreversibility of the time series to quantify the nonequilibrium of the system. The data of long-time trajectories of X and Y simulated from the

Langevin equation with the noise induced attractor switching between *Macroalgae* and *Coral*. The cross correlation function forward in time is defined as follows: $C_{XY}(\tau) = \langle X(0)Y(\tau) \rangle$, where X and Y denote the time trajectories of the variables X and Y with time interval τ ^{42,43}. $\tilde{C}_{XY}(\tau)$ represents the cross correlation function backward in time. Thus, the average difference in cross correlations between the forward in time and the backward in time, can be used to quantify the time irreversibility. It is defined as $\Delta CC = \sqrt{\frac{1}{t_f} \int_0^{t_f} (C_{XY}(\tau) - \tilde{C}_{XY}(\tau))^2 d\tau}$. The cross correlation difference can quantify the degree of nonequilibrium and measure the strength of the flux due to the time irreversibility, which is related to the degree of the detailed balance breaking^{42–44}. It provides a practical way for the indicator of the phase transitions and bifurcations for the coral-algal system directly from the observed temporal trajectory. In this study, we calculate the time irreversibility quantified by the difference in the forward cross correlation in time and backward one ΔCCM (the system stays in state *Macroalgae*) and ΔCCC (the system stays in state *Coral*) using a relatively small diffusion coefficient in order to avoid jumping between the steady-state states. This means that when the system stays at the state *Macroalgae* at first, then under a relative small diffusion coefficient D , it is hard to jump to the alternative state *Coral*. Thus, we can collect enough stochastic simulated data which the system stays in the state *Macroalgae* without having the possibility of the trajectory jumping to the state *Coral*. Once the system jumps to *Coral*, a phase transition cannot be predicted in advance by ΔCCM , since the alternative state has appeared already.

ΔCCM (for state *Macroalgae*) and ΔCCC (for state *Coral*) versus g shown in Figure 8A both have a peak between the two transcritical bifurcations with small fluctuations ($D = 1 \times 10^{-5}$) and $h = 0.44$. We show $k_{\Delta CCM}$ (the slope of ΔCCM) versus g and $kk_{\Delta CCM}$ (the slope of $k_{\Delta CCM}$) versus g for state *Macroalgae* and $k_{\Delta CCC}$ (the slope of ΔCCC) versus g and $kk_{\Delta CCC}$ (the slope of $k_{\Delta CCC}$) versus g for state *Coral* in Figure 8BC. We used the exponential function to fit the data from simulations to calculate the slope of the lines. We can see that $k_{\Delta CCM}$, $kk_{\Delta CCM}$, $k_{\Delta CCC}$ and $kk_{\Delta CCC}$ have their inflection points,

which denote that they have significant changes approaching the bifurcation.

Critical slowing down can appear when the ecosystem is close to the edges of bifurcation points in the case of gradual changes in external environmental conditions. When a system in a stable basin is subjected to external disturbance, it will return to its original stable state after a period of time, which is called the relaxation time¹¹. This relaxation time can be interpreted as the time it takes for the system to adapt to changes in the environment. In Figure 8D, we see that the relaxation time τ_{relaxM} for state *Macroalgae* has a sharp increase near the right bifurcation, and the relaxation time τ_{relaxC} for the state *Coral* has a sharp increase near the left bifurcation with small fluctuations ($D = 1 \times 10^{-5}$). We show k_{CSDM} (the slope of the relaxation time τ_{relaxM}), k_{CSDC} (the slope of the relaxation time τ_{relaxC}), kk_{CSDM} (the slope of the k_{CSDM}) and kk_{CSDC} (the slope of the k_{CSDC}) versus grazing rate g in Figure 8EF. We can see that the slopes $k_{\Delta CCC}$ and $kk_{\Delta CCC}$ both have sharp increases, which means that the τ_{relax} increases approaching the bifurcation. In comparison, our nonequilibrium warning indicators (flux, entropy production rate, time irreversibility) provide much earlier predictions for the bifurcations than those from the critical slowing down indicators. For example, the peaks in ΔCCC and ΔCCM in Figure 8 A occur within the bistable zone, while the peaks in τ_{relax} in Figure 8 D occur right at the bifurcation points. This point is further illustrated in Figure 9 where we vary both the grazing rate g and the natural mortality rate of coral h ; we always observe that the peaks of the landscape-flux indicators occur further from the bifurcation points than the CSD indicators.

The non-equilibrium driving force quantified by the flux, the thermodynamic cost quantified by EPR , the intrinsic free energy and time irreversibility all can be seen as the early warning signals, which are far earlier than the prediction of the currently available methods. These non-equilibrium early warning signals can provide indicators for predicting bifurcation/phase transition to avoid catastrophic phase transition. In the coral reef model we studied here, we predicted the transition from the regime in which the dominant state of the *Macroalgae* state to the dominant state of the *Coral* state in the middle of the two stable state coexistence range, rather than approaching to the $g = 0.3927$ level where the *Coral* state is becoming dominant. This led to a much earlier warning signal than have been previously reported^{12–14}.

As we vary the grazing rate g , there are two directions from which we can approach the bifurcations: the increasing g direction and the decreasing g direction. Critical slowing down can identify the left bifurcation where the *Macroalgae* attractor state becomes dominant and the *Coral* attractor state becomes flat (the left transcritical bifurcation) in the decreasing g direction and the right bifurcation where the *Coral* attractor state becomes dominant and the *Macroalgae* attractor state becomes flat (the right transcritical bifurcation) in the increasing g direction. We can see that both the relaxation time and the switching frequency increase sharply in increasing g direction when approaching towards the right

transcritical bifurcation as shown in Figure 8D while the relaxation time increase sharply in the decreasing g direction when approaching towards the left transcritical bifurcation as shown in Figure 8D.

We can clearly see that our nonequilibrium warning indicators in terms of the flux, the entropy generation rate, the time irreversibility from the cross correlation of the observed time series and the non-equilibrium free energy are located between the two transcritical bifurcations. Our nonequilibrium warning signals are earlier than the right bifurcation (indicated from the critical slowing down) from the perspective of the current *Macroalgae* state where one is at (*Macroalgae* state becomes flat and unstable while *Coral* state becomes dominant). On the other hand, our nonequilibrium warning signals are earlier than the left bifurcation (indicated from the critical slowing down) from the perspective of the current *Coral* state where one is at (*Coral* state becomes flat and unstable while *Macroalgae* state becomes dominant). Thus, our indicators, whose turning points are in the middle of two bifurcations, can provide the predictions for both left bifurcation and right bifurcation and they are much earlier than the predictions given by the critical slowing down which are all near the bifurcation.

The results from the critical slowing down will miss one bifurcation in each direction, for example, as the parameter g increases towards the right bifurcation, the left transcritical bifurcation will be missed where the current *Macroalgae* attractor state dominates (left transcritical bifurcation in the phase diagram), while the *Coral* attractor state just appears and is shallow. This is because the critical slowing down will only emerge when the landscape around the current attractor state becomes flat as the parameter approaches the right bifurcation. When the right bifurcation appears in the prospective *Coral* attractor state, the current attractor *Macroalgae* state in which the system is located becomes flat, resulting in a critical slowing down. However, when the current *Macroalgae* state approaches the left bifurcation point, it becomes dominant to other states, but the related landscape around the current *Macroalgae* state is not flat. Thus, it is not expected that there will be any critical slowing down near the left bifurcation point in the increasing g direction. Therefore, when the current *Macroalgae* attractor state dominates, the critical slowing down cannot be used to predict the left bifurcation in the increasing g direction, and similarly when the current *Coral* attractor state dominates, the critical slowing down cannot be used to predict the right bifurcation in the decreasing g direction.

The non-equilibrium early warning signals appearing in the middle of the two bifurcations are much earlier for both directions than the critical slowing down indicators, appearing near the left bifurcation in the decreasing g direction and near the right bifurcation in the increasing g direction. Our non-equilibrium early warning signals have a clear advantage that we can predict both the left and right bifurcations (much earlier than the critical slowing down for both bifurcations by sitting at different attractor states), which is shown in Figure 2BC and Figure 7.

Critical slowing down has been widely used in models

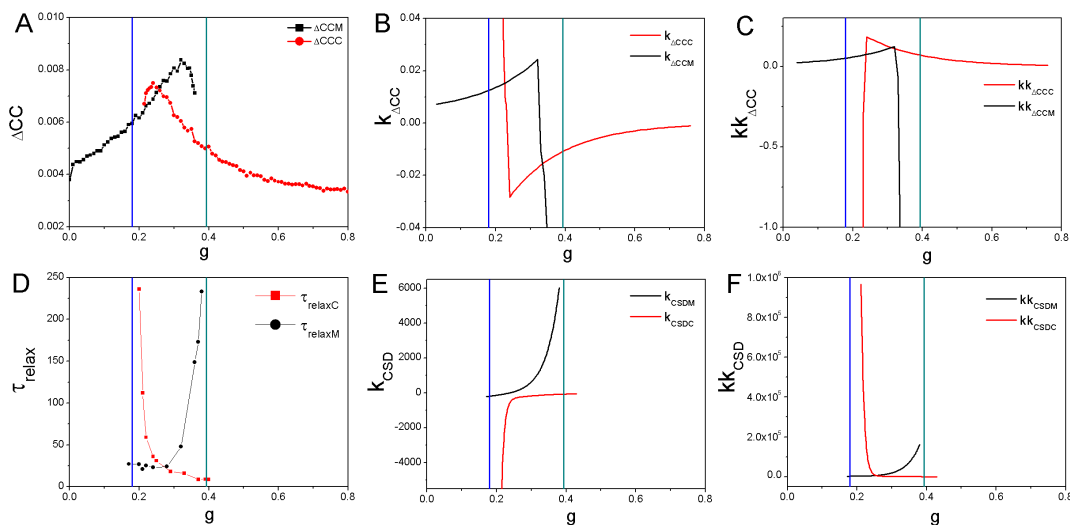


FIG. 8. A: The average difference of the cross correlations forward and backward in time ΔCCM and ΔCCC versus g . B: $k_{\Delta CCM}$ (the slope of ΔCCM) and $k_{\Delta CCC}$ (the slope of ΔCCC) versus g . C: $kk_{\Delta CCM}$ (the slope of $k_{\Delta CCM}$) and $kk_{\Delta CCC}$ (the slope of $k_{\Delta CCC}$) versus g . D: The relaxation time τ_{relaxM} and τ_{relaxC} versus grazing rate g . E: k_{CSDM} (the slope of the relaxation time τ_{relaxM}) and k_{CSDC} (the slope of the relaxation time τ_{relaxC}) versus grazing rate g . F: kk_{CSDM} (the slope of the k_{CSDM}) and kk_{CSDC} (the slope of the k_{CSDC}) versus grazing rate g . ($h = 0.44$)

with saddle-node bifurcations. In our case, because the stable solutions leave the feasible region exactly at the point at which transcritical bifurcations occur, we effectively have the same qualitative dynamics that occur in models with saddle-node bifurcations. In particular, there is one stable and one unstable solution approaching the bifurcation and both solutions disappear after the bifurcation occurs. So far, most studies have been focused on effective one-dimensional methods, the results of which can often be applied to effective equilibrium systems where global stability can be quantified by landscape alone, without considering the key non-equilibrium ingradient component, i.e., flux^{11–14}. Our fully vectorized high dimensional formulation of the potential-flux landscape can quantify the non-equilibrium by the non-zero curl flux, which can lead to a much richer complex dynamics with detailed balance breaking. In contrast, the equilibrium dynamics are determined entirely by the gradient of the potential landscape. Curl fluxes that break the detailed equilibrium play an important role in driving the dynamics of the non-equilibrium system.

Figure 9 shows the two-parameter phase diagram of the natural mortality rate of corals h versus grazing rate g for the coral-algal model. There are four regions with different colors, which denote different phases, separated by several curves of bifurcation points (curves of transcritical points in black, curve of saddle node points in blue). In the blue region, only the "Macroalgae" state is stable, while both the "Macroalgae" and "Coral" states are stable in the grey region. In the purple region, only the "Coral" state is stable, while there are no feasible stable states in the pink region. And we show the phase diagram for different h in Figure S2.

Figure 10 shows the EPR and $Flux_{av}$ versus grazing rate g with different natural mortality rate of corals h for the coral-algal model, and Figure S3 shows the EPR (A,B,C,D)

and $Flux_{av}$ (E,F,G,H) versus grazing rate g with different natural mortality rate of corals h for the coral-algal model respectively. We can see that there is a peak in each data curve in its corresponding bistable region, which denotes that EPR and $Flux_{av}$ can be viewed as the indicators for the phase transitions.

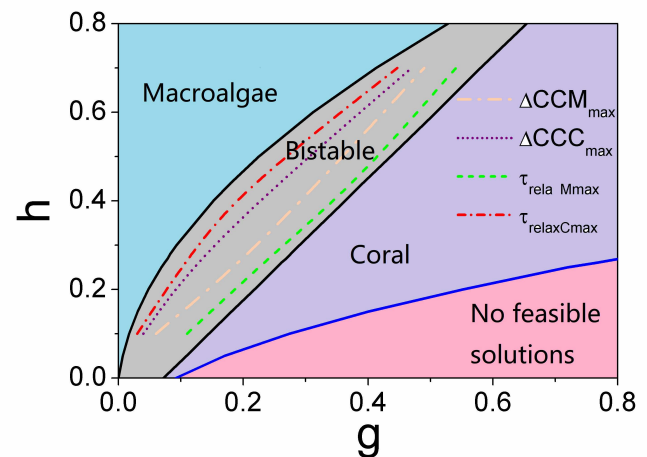


FIG. 9. The two-dimensional phase diagram of the natural mortality rate of corals h versus grazing rate g for the coral-algal model. ΔCCM_{max} represents the maximum of ΔCCM , ΔCCC_{max} represents the maximum of ΔCCC . $\tau_{relaxMmax}$ represents the coordinate position of the sharp rise of τ_{relaxM} , $\tau_{relaxCmax}$ represents the coordinate position of the sharp rise of τ_{relaxC} .

Figure 11 ($h = 0.3$) and Figure S4 ($h = 0.7$) show that the time irreversibility quantified by the difference in the forward cross correlation in time and backward one ΔCCM (for state *Macroalgae*) and ΔCCC (for state *Coral*) versus g shown in

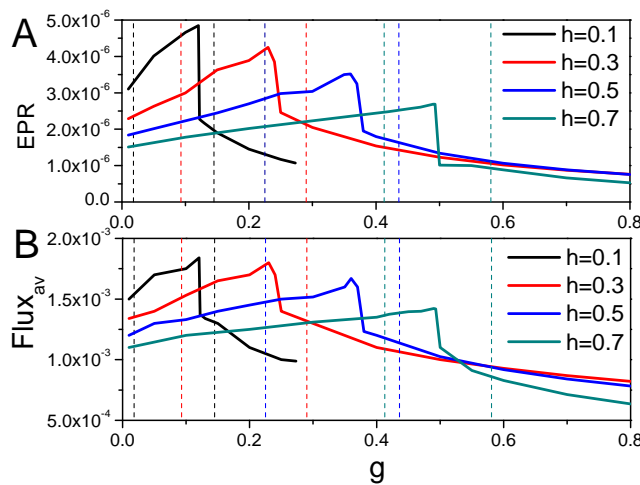


FIG. 10. The EPR and $Flux_{av}$ versus grazing rate g with different natural mortality rate of corals h for the coral-algal model. The dashed lines represent the locations of the transcritical points for each value of h with the same color for the EPR lines.

each subfigure A have a peak between the two transcritical bifurcations with small fluctuations ($D = 1 \times 10^{-5}$). We show $k_{\Delta CCM}$ (the slope of ΔCCM) versus g and $kk_{\Delta CCM}$ (the slope of $k_{\Delta CCM}$) versus g for state *Macroalgae* and $k_{\Delta CCC}$ (the slope of ΔCCC) versus g and $kk_{\Delta CCC}$ (the slope of $k_{\Delta CCC}$) versus g for state *Coral* in each subfigure BC. We can see that $k_{\Delta CCM}$, $kk_{\Delta CCM}$, $k_{\Delta CCC}$ and $kk_{\Delta CCC}$ have their inflection points, which denote that they have significant change approaching to the bifurcation. In each subfigure C, we see that the relaxation time τ_{relaxM} for state *Macroalgae* has a sharp increase near the right bifurcation, and the relaxation time τ_{relaxC} for state *Coral* has a sharp increase near the left bifurcation with small fluctuations ($D = 1 \times 10^{-5}$). We show k_{CSDM} (the slope of the relaxation time τ_{relaxM}), k_{CSDC} (the slope of the relaxation time τ_{relaxC}), kk_{CSDM} (the slope of the k_{CSDM}) and kk_{CSDC} (the slope of the k_{CSDC}) versus grazing rate g in each subfigure EF. We can see that the slope $k_{\Delta CCC}$ and $kk_{\Delta CCC}$ both have sharp increases, which denote that the τ_{relax} increases significantly approaching to the bifurcation.

We can see that ΔCCM_{max} representing the coordinate position of the maximum of ΔCCM , ΔCCC_{max} representing the coordinate position of the maximum of ΔCCC , $\tau_{relaxMmax}$ representing the coordinate position of the sharp rise of τ_{relaxM} and $\tau_{relaxCmax}$ representing the coordinate position of the sharp rise of the maximum of τ_{relaxC} (We set the $kk > 1 \times 10^4$ as the sharp rise position) are in the bistable region. The line $\tau_{relaxMmax}$ is much nearer to the right bifurcation line (red) than the line ΔCCM_{max} , while the line $\tau_{relaxCmax}$ is much nearer to the left bifurcation line (black) than the line ΔCCC_{max} . Thus, ΔCC is earlier warning signal than the τ_{relax} . These results all show that ΔCC can be used as an good indicator of early warning signal.

IV. CONCLUSION

We investigated the global dynamics of a well-known coral-algal model subject to stochastic forcing using the landscape-flux theory from non-equilibrium statistical physics. The dynamics of coral-algal ecological systems are determined by the potential landscapes and the curl flux; the potential landscape attracts the system towards the potential minimum while the curl fluxes drives the dynamics between the states. It is crucial to quantify the stability of an ecological system and global stability can be quantified by an appropriate Lyapunov function, which is difficult to obtain for complex ecological systems. The underlying intrinsic potential landscape ϕ_0 provided by our general method is a Lyapunov function in the small noise limit and hence can be used to quantify the global stability of the coral-algal system.

Due to the presence of non-zero fluxes, the dominant paths describing how the system switches between alternative stable states do not simply follow the expected steepest descent paths based on the population-potential landscape. The dominant paths from *Macroalgae* to *Coral* and vice versa are irreversible, i.e. depend on the direction of the transition, and are determined by the underlying population-potential landscape and the flux; the origin of the path irreversibility is the non-zero curl flux.

Even in the bistable regime, the basin of attraction of the current state is not completely flat until the right bifurcation point. Thus, if the noise is small enough, one can still predict the upcoming of the impending state transition. This is because, on a finite time interval, the small fluctuations are not enough to drive the state switching to another one until to the right bifurcation, where the current state becomes completely flat and the other basin becomes dominant. Therefore, the peak of the time irreversibility from the difference in cross correlation forward and backward in time is generated by the stochastic trajectories staying in the current state basin without jumping to another one even in the bistable regime. Hence one can use that as a predictor for the bifurcation on the right for the new state to become dominant.

We found that barrier heights between the stable states, the kinetic switching time as mean first passage time $MFPT$, the thermodynamic cost as entropy production rate EPR , and the dynamical driving force as average flux can be used as quantitative markers for the stability and dynamics of the coral-algal system. We found that the average flux $Flux_{av}$, the entropy production rate EPR and the intrinsic average flux $inFlux_{av}$, the intrinsic entropy production rate $inEPR$ have the same trends. The flux due to its rotational nature always tends to destabilize the point attractor. This provides the dynamical origin for the phase transitions or bifurcations of coral-algal ecosystem. To maintain the non-equilibrium flux, there is a dissipation cost associated. Thus the non-equilibrium instability or bifurcation requires energy cost. This provides the thermodynamics origin of phase transition or bifurcations of coral-algal ecosystem. The intrinsic free energy is also a marker for early warning signal. Their significant changes and peaks are between the two transcritical bifurcations. It is even more significant for the intrinsic potential landscapes

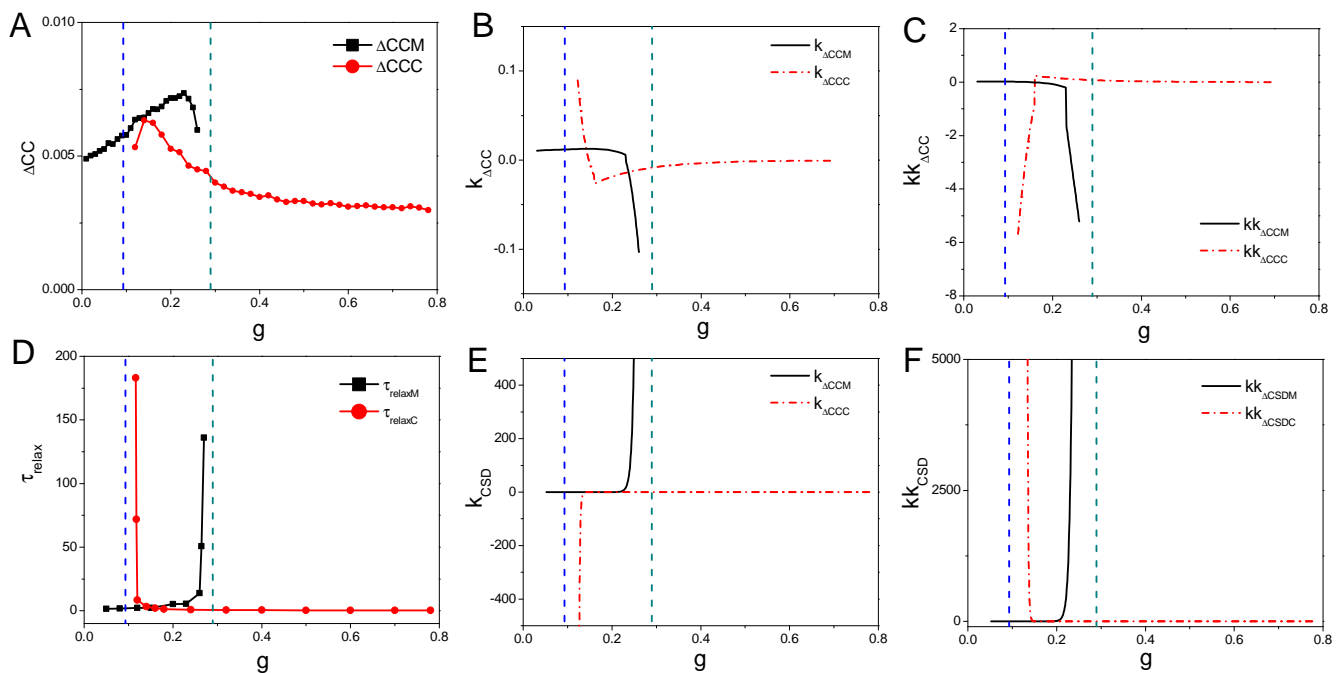


FIG. 11. $h = 0.3$ A: The average difference of the cross correlations forward and backward in time ΔCCM (for state *Macroalgae*) and ΔCCC (for state *Coral*) versus g . B: $k_{\Delta CCM}$ (the slope of ΔCCM) and $k_{\Delta CCC}$ (the slope of ΔCCC) versus g . C: $kk_{\Delta CCM}$ (the slope of $k_{\Delta CCM}$) and $kk_{\Delta CCC}$ (the slope of $k_{\Delta CCC}$) versus g . D: The relaxation time τ_{relaxM} and τ_{relaxC} versus grazing rate g . E: k_{CSDM} (the slope of the relaxation time τ_{relaxM}) and k_{CSDC} (the slope of the relaxation time τ_{relaxC}) versus grazing rate g . F: kk_{CSDM} (the slope of the k_{CSDM}) and kk_{CSDC} (the slope of the k_{CSDC}) versus grazing rate g .

with zero fluctuation limit.

Our nonequilibrium early warning indicators with the average flux $Flux_{av}$, the entropy production rate EPR , the time irreversibility from the cross correlation of the observed time series ΔCC and the non-equilibrium free energy can all be used as the predictors for the critical transitions. We can see that their turning points (the peaks or the troughs) are all located between the two transcritical bifurcations. Our indicators can predict both bifurcations before the current state becomes flat. The nonequilibrium warning signals we propose are earlier than the right bifurcation from the current *Macroalgae* state in the increasing g direction, while our nonequilibrium warning signals are earlier than the left bifurcation from the current *Coral* state in the decreasing g direction. Thus, the nonequilibrium warning indicators can provide earlier warnings than the CSD theory for both the left bifurcation and right bifurcations. Different models will lead to different locations of the tipping points^{30,31}, but we believe that the turning points of the non-equilibrium indicators lying between the two transcritical bifurcations is a generic feature of systems with similar qualitative dynamics.

While the model studied there is primarily phenomenological and neglects many features of real-world coral reef systems, it allows us to illustrate the power of the landscape-flux method for developing early warning signals of critical transitions. Moreover, the results presented here are a first step in adapting our methods to tackle more complex and realistic ecosystem models. We intend to explore

more complex coral reef models in subsequent research and this will include addressing important features omitted from the present study, such as recruitment seasonality, grazing influence and explicit spatial extent^{7,8}.

Coral degradation and coral reef ecological environment deterioration are pressing conservation challenges. The theoretical study of coral reef ecosystem can provide effective guidance for the protection and restoration of these and other threatened ecological systems.

ACKNOWLEDGMENTS

LX thanks supports by Natural Science Foundation of Jilin Province No. 20220101013JC and National Natural Science Foundation of China No.12234019. SL and DP appreciate support from NSF DMS-1951358.

- ¹J. W. Mcmanus and J. F. Polsenberg, "Coral-algal phase shifts on coral reefs: ecological and environmental aspects," *Progress in Oceanography* **60**, p.263–279 (2004).
- ²T. P. Hughes, M. J. Rodrigues, D. R. Bellwood, D. Ceccarelli, O. Hoegh-Guldberg, L. Mccook, N. Moltschaniwskyj, M. S. Pratchett, R. S. Steneck, and B. Willis, "Phase shifts, herbivory, and the resilience of coral reefs to climate change," *Current Biology* **17**, 360–365 (2007).
- ³L. J. Mccook, J. Jompa, and G. Diaz-Pulido, "Mccook l, jompa j, diaz-pulido g.. competition between corals and algae on coral reefs: a review of evidence and mechanisms. coral reef 19: 400–417," *Coral Reefs* **19** (2001).
- ⁴S. R. Dudgeon, R. B. Aronson, J. F. Bruno, and W. F. Precht, "Phase shifts and stable states on coral reefs," *Marine Ecology Progress Series* **413**, 201–216 (2010).

- ⁵P. J. Mumby, A. Hastings, and H. J. Edwards, "Thresholds and the resilience of caribbean coral reefs," *Nature* **450**, 98–101 (2007).
- ⁶X. Li, H. Wang, Z. Zhang, and A. Hastings, "Mathematical analysis of coral reef models," *Journal of Mathematical Analysis and Applications* **416**, 352–373 (2014).
- ⁷L. C. McManus, J. R. Watson, V. V. V., and S. A. Levin, "Stability and recovery of coral-algae systems: the importance of recruitment seasonality and grazing influence," *Theoretical Ecology* **12**, 61–72 (2018).
- ⁸V. Nes, H. Egbert, V. D. Leemput, A. Ingrid, Hughes, P. Terry, and M. Scheffer, "Multiple feedbacks and the prevalence of alternate stable states on coral reefs," *Coral reefs:journal of the International Society for Reef Studies* **35**, 857–865 (2016).
- ⁹A. Diko, "Ecological processes and contemporary coral reef management," *Diversity* **2**, 717–737 (2010).
- ¹⁰J. M. Pandolfi, R. H. Bradbury, E. Sala, T. P. Hughes, A. Karen, R. G. Cooke, D. Mcardle, L. Mcclenachan, M. J. H. Newman, and G. Paredes, "Global trajectories of the long-term decline of coral reef ecosystems," *Science* **301**, 955–958 (2003).
- ¹¹M. Scheffer, J. Bascompte, W. A. Brock, V. Brovkin, S. R. Carpenter, V. Dakos, H. Held, E. Nes, M. Rietkerk, and G. Sugihara, "Early-warning signals for critical transitions," *Nature* **461**, 53–9 (2009).
- ¹²A. J. Veraart, E. J. Faassen, V. Dakos, E. Nes, M. Liirling, and M. Scheffer, "Recovery rates reflect distance to a tipping point in a living system," *Nature* **481**, 357–359 (2012).
- ¹³M. Scheffer, S. Carpenter, J. A. Foley, C. Folke, and B. Walker, "Catastrophic shifts in ecosystems," *Nature* **413**, 591–596 (2001).
- ¹⁴M. Scheffer, S. R. Carpenter, T. M. Lenton, J. Bascompte, W. Brock, V. Dakos, J. Koppel, I. Leemput, S. A. Levin, and E. Nes, "Anticipating critical transitions," *Science* **338**, 344 (2012).
- ¹⁵A. Hastings, A. Karen C., K. Cuddington, T. Francis, G. Gellner, Y. Lai, A. Morozov, S. Petrovskii, K. Scranton, and M. Zeeman, "Transient phenomena in ecology," *Science* **361**, eaat6412 (2018).
- ¹⁶C. Boettiger and A. Hastings, "From patterns to predictions," *Nature* **493**, 157–158 (2013).
- ¹⁷C. Boettiger, R. N., and A. Hastings, "Early warning signals: the charted and uncharted territories," *Theor. Ecol.* **6**, 255–264 (2013).
- ¹⁸B. C. Nolting and K. C. Abbott, "Balls, cups, and quasi-potentials: quantifying stability in stochastic systems," *Ecology* **97**, 850–864 (2016).
- ¹⁹K. A. Lamothe, K. M. Somers, and D. A. Jackson, "Linking the ball-and-cup analogy and ordination trajectories to describe ecosystem stability, resistance, and resilience," *Ecosphere* **10**, e02629 (2019).
- ²⁰K. C. Abbott and V. Dakos, "Mapping the distinct origins of bimodality in a classic model with alternative stable states," *Theoretical Ecology* **14**, 673–684 (2021).
- ²¹L. Xu, K. Zhang, and J. Wang, "Exploring the mechanisms of differentiation, dedifferentiation, reprogramming and transdifferentiation," *PLoS ONE* **9**, e105216 (2014).
- ²²J. Wang, "Landscape and flux theory of non-equilibrium dynamical systems with application to biology," *Advances in Physics* **64**, 1–137 (2015).
- ²³J. Wang, L. Xu, and E. K. Wang, "Potential landscape and flux framework of nonequilibrium networks: Robustness, dissipation, and coherence of biochemical oscillations," *Proc Natl Acad Sci USA* **105**, 12271–12276 (2008).
- ²⁴L. Xu, H. Shi, H. Feng, and J. Wang, "The energy pump and the origin of the non-equilibrium flux of the dynamical systems and the networks," *J. Chem. Phys.* **136**, 165102 (2012).
- ²⁵J. Wang, K. Zhang, L. Xu, and E. Wang, "Quantifying the waddington landscape and biological paths for development and differentiation," *Proc Natl Acad Sci USA* **108**, 8257–8262 (2011).
- ²⁶J. Wang, L. Xu, and E. K. Wang, "The potential landscape of genetic circuits imposes the arrow of time in stem cell differentiation," *Biophys. J.* **99**, 29–39 (2010).
- ²⁷H. Qian, "Open-system nonequilibrium steady-state: Statistical thermodynamics, fluctuations and chemical oscillations," *J Phys Chem B* **110**, 15063–15074 (2006).
- ²⁸H. Ge and H. Qian, "The physical origins of entropy production, free energy dissipation and their mathematical representations," *Phys. Rev. E* **81**, 051133 (2010).
- ²⁹H. Qian, "Entropy demystified: The "thermo"-dynamics of stochastically fluctuating systems," *Method Enzymol* **467**, 111–134 (2009).
- ³⁰L. Xu, D. Patterson, A. Staver, S. Levin, and J. Wang, "Unifying deterministic and stochastic ecological dynamics via a landscape-flux approach," *Proc. Natl. Acad. Sci. U.S.A.* **118**, e2103779118 (2021).
- ³¹L. Xu, D. Patterson, S. Levin, and J. Wang, "Non-equilibrium early-warning signals for critical transitions in ecological systems," *Proc. Natl. Acad. Sci. U.S.A.* **120**, e2218663120 (2023).
- ³²D. Gillespie, "Exact stochastic simulation of coupled chemical reactions," *J Phys Chem* **81**, 2340–2361 (1977).
- ³³P. Swain, M. Elowitz, and E. Siggia, "Intrinsic and extrinsic contributions to stochasticity in gene expression," *Proc Natl Acad Sci USA* **99**, 12795–12800 (2002).
- ³⁴N. Van Kampen, *Stochastic processes in physics and chemistry* (Elsevier, Amsterdam, 2007).
- ³⁵G. Nicolis and I. Prigogine, *Self-organization in nonequilibrium systems* (Wiley, New York, 1977).
- ³⁶H. Qian, "Open-system nonequilibrium steady-state: Statistical thermodynamics, fluctuations and chemical oscillations," *J Phys Chem B* **110**, 15063–15074 (2006).
- ³⁷F. Zhang, L. Xu, K. Zhang, E. Wang, and J. Wang, "The potential and flux landscape theory of evolution," *J. Chem. Phys.* **137**, 065102 (2012).
- ³⁸H. Ge and H. Qian, "The physical origins of entropy production, free energy dissipation and their mathematical representations," *Phys. Rev. E* **81**, 051133 (2010).
- ³⁹L. Xu, F. Zhang, K. Zhang, E. K. Wang, and J. Wang, "The potential and flux landscape theory of ecology," *PLoS ONE* **9**, e86746 (2014).
- ⁴⁰M. Scheffer, S. Hosper, M.-L. Meijer, B. Moss, and E. Jeppesen, "Alternative equilibria in shallow lakes," *Trends in Ecology and Evolution* **8**, 275–279 (1993).
- ⁴¹M. Scheffer, *Critical Transitions in Nature and Society* (Princeton University Press, Princeton, 2009).
- ⁴²H. Qian and E. Elson, "Fluorescence correlation spectroscopy with high-order and dual-color correlation to probe nonequilibrium steady state," *Proc Natl Acad Sci U S A* **101**, 2828–2833 (2004).
- ⁴³K. Zhang and J. Wang, "Exploring the underlying mechanisms of the xenopus laevis embryonic cell cycle," *J. Phys. Chem. B* **122**, 5487–5499 (2018).
- ⁴⁴L. Xu and J. Wang, "Curl flux as a dynamical origin of the bifurcations/phase transitions of nonequilibrium systems: Cell fate decision making," *J. Phys. Chem. B* **124**, 2549–2559 (2020).